

Journal of Biomedical Optics

SPIEDigitalLibrary.org/jbo

Effect of object size and acoustic wavelength on pulsed ultrasound modulated fluorescence signals

Nam T. Huynh
Haowen Ruan
Diwei He
Barrie R. Hayes-Gill
Stephen P. Morgan

Effect of object size and acoustic wavelength on pulsed ultrasound modulated fluorescence signals

Nam T. Huynh, Haowen Ruan, Diwei He, Barrie R. Hayes-Gill, and Stephen P. Morgan

University of Nottingham, Electrical Systems and Optics Research Division, Faculty of Engineering, Nottingham, United Kingdom

Abstract. Detection of ultrasound (US)-modulated fluorescence in turbid media is a challenge because of the low level of fluorescent light and the weak modulation of incoherent light. A very limited number of theoretical and experimental investigations have been performed, and this is, to our knowledge, the first demonstration of pulsed US-modulated fluorescence tomography. Experimental results show that the detected signal depends on the acoustic frequency and the fluorescent target's size along the ultrasonic propagation axis. The modulation depth of the detected signal is greatest when the length of the object along the acoustic axis is an odd number of half wavelengths and is weakest when the object is an integer multiple of an acoustic wavelength. Images of a fluorescent tube embedded within a 22- by 13- by 30 mm scattering gel phantom ($\mu_s \sim 15 \text{ cm}^{-1}$, $g = 0.93$) with 1-, 1.5-, and 2 MHz frequency US are presented. The modulation depth of the detected signal changes by a factor of 5 depending on the relative size of the object and the frequency. The approach is also verified by some simple experiments in a nonscattering gel and using a theoretical model. © 2012 Society of Photo-Optical Instrumentation Engineers (SPIE). [DOI: 10.1117/1.JBO.17.7.076008]

Keywords: ultrasound-modulated fluorescence tomography; scattering.

Paper 12052P received Jan. 25, 2012; revised manuscript received May 25, 2012; accepted for publication Jun. 1, 2012; published online Jul. 6, 2012.

1 Introduction

Labeling living cells using fluorescent dye is widely used in the life sciences, as it provides physiological information of tissue and its microenvironment.¹ For three-dimensional (3-D) cell culture and animal studies, however, light scattering presents a problem. Although imaging techniques such as confocal microscopy and multiphoton microscopy can reduce the effects of light scattering, the penetration depth is typically 500 μm in tissues such as skin. It would therefore be extremely useful to develop techniques for imaging fluorescence in tissues >1 mm thick in three dimensions, while maintaining relatively high spatial resolution.

Some research has been carried out using multiwavelength photo-acoustic tomography,^{2,3} although this relies on light absorption by the fluorophores rather than direct measurement of the fluorescent light itself, and therefore interpretation of the results may be difficult in the presence of multiple absorbers. Ultrasound-modulated optical tomography (USMOT) has the potential to directly image fluorescence in scattering media. In general, a focused ultrasound (US) beam acts as a scanning probe within the illuminated optically scattering samples. The scattered light at the US focus is modulated and then detected at the photo detector. The detected signal carries information that can be analyzed to provide information about the optical properties of the sample at the US focus. This hybrid method provides the ability to image targets embedded deeply within turbid media (e.g., tissues) with optical contrast and US resolution.⁴ Coherent light has conventionally been used in USMOT,⁵⁻⁹ as the refractive index change and motion of scatterers induced

by the US produces a modulated speckle pattern that can be used to improve signal to noise ratio (SNR).

US-modulated fluorescence tomography (USMFT) involves detection of incoherent light,¹⁰ which means that the detected modulated signals are significantly lower. A fairly limited amount of research has been conducted in this area. Much of this has been fundamental, investigating the mechanisms for modulation¹⁰⁻¹⁴ and concentrating on the position of the US focus relative to the fluorescent target. For example, Yuan and colleagues^{10,14} and Hall¹² suggested that modulating the excitation beam would be most effective. This contradicted work by Kobayashi et al.,¹¹ who demonstrated that the modulated optical signal was greatest when the US focus was at the fluorescent object. The model by Krishnan et al.¹³ predicted that the maximum modulation strength of fluorescence signals would occur when the US focus was close to the fluorescent molecules or the detector. This has yet to be resolved, and will not be the focus of this paper. Hall et al.¹⁵ and Honeysett et al.¹⁶ showed an improvement in USMOT imaging in the presence of contrast agents (microbubbles) due to a greater change in the optical properties in the presence of insonified bubbles. Other work has proposed the use of bubbles comprising fluorophore and quencher^{10,17,18} that produce fluorescent signals in the presence of US but are quenched in its absence.

To date, continuous wave (CW) US has been employed in all USMFT systems. There are several advantages of using pulsed US. As in conventional US, depth-resolved imaging along the US axis can be achieved by time-gating the detection. Furthermore, because of maximum permissible exposure regulations, CW excitation restricts the instantaneous power that can be applied to tissue. Low instantaneous power from

Address all correspondence to: Stephen P Morgan, Prof. of Biomedical Engineering, Faculty of Engineering, University of Nottingham, NG7 2RD, United Kingdom. Tel: +44 (0)115 9515570; E-mail: Steve.morgan@nottingham.ac.uk

the transducer also leads to a low-modulation-depth signal. An important aspect for the detection of low-light-level, low-modulation-depth USMFT signals is that electromagnetic radiation (EMR) from the RF power amplifier or the US transducer can often be picked up at the detector side (photodetector, electronic filters, and amplifiers).^{14,19} Consequently, it appears as a background signal at the US frequency in the detected data. This implies that even when there is no modulated fluorescence, a signal can still be observed at the ultrasonic frequency, and when there is modulated fluorescence present, the two detected electrical signals interfere with each other and can produce a reduction in the detected intensity.^{14,19} With pulse or tone-burst excitation, the EMR effect is avoided because the modulated optical signal is detected at a delayed time after the excitation pulse. This delay is the propagation time of an US pulse from the transducer surface to its focal zone in the medium.

To our knowledge, we present the first pulsed USMFT system in this paper. The effects of the acoustic frequency and the fluorescent target's size along the ultrasonic axis were investigated, and the magnitude of the detected signal was shown to be highly dependent on these parameters. Initial verification of this effect was carried out using nonscattering samples and also a simple numerical model^{20,21} of the generation and propagation of US-modulated fluorescent pulses in the medium. This was further confirmed by experiments in a scattering medium.

The next section discusses the simple theoretical model of a pulsed/tone-burst USMFT. Section 3 gives the details of the experimental configurations. The results for different targets in clear water and a scattering gel are presented in Sec. 4. Discussion and conclusions follow in Secs. 5 and 6, respectively.

2 Theory

In the experimental system (Sec. 3), US is focused in front of the fluorescent target to avoid distortion of the acoustic focal region due to an acoustically inhomogeneous target. Other work^{10–12} has noted that the highest US-modulated fluorescence signal can be achieved with this configuration. The simple simulation developed reflects this configuration; excitation light is modulated by the US, which then excites the fluorophore and produces modulated fluorescence. The shape of the US excitation pulse is imposed on the temporal profile of the modulated fluorescence.

We have previously demonstrated that the shape of the temporal signal produced in a pulsed USMOT experiment

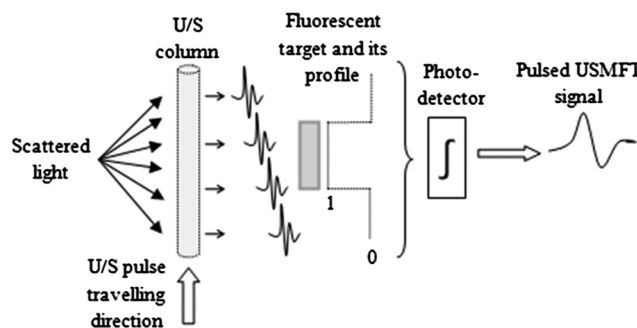


Fig. 1 Pulsed USMFT model showing a target with a flat fluorescent profile.

can be predicted by convolution of the optical profile along the optical axis with the acoustic pulse that propagates along the axis (Fig. 1). A detailed explanation can be found elsewhere,^{20,21} and so only the adaptations necessary to take into account fluorescence signals are described here. As an ultrasonic pulse traverses the sample, at a particular time, it introduces a pressure change (compression or rarefaction) at a particular volumetric element of the medium, which contains the ultrasonic pressure at a given point in time (defined as a “layer” in this context). This modulates the motion of local scatterers and changes the local sample’s optical properties (scattering coefficient, absorption coefficient, and refractive index). Consequently, light at that layer is phase-modulated by the ultrasonic pulse and produces an optical pulse. When the ultrasonic pulse reaches the next layer of the sample, it produces another optical pulse, which is similar to the temporal pulse from the previous layer but with a phase delay due to the time taken for the ultrasonic pulse to propagate between the two consecutive layers. The speed of sound v_a in water and in gel phantoms²² has been demonstrated to be approximately 1500 m/s at room temperature. The speed of light v in such media is expressed as $v = c/n$, where $c \approx 3 \times 10^8$ m/s is the light velocity in vacuum and $n \approx 1.33$ is the refractive index of water or tissue. As the speed of light is much higher than the speed of sound, the time taken for the modulated light to reach the fluorescent region (placed next to the US focal region) is neglected. Hence, the phase difference depends only on the transit time of the ultrasonic pulse, which produces a slowly changing envelope on the modulated signal. Pulsed excitation light (to the fluorescent target) may be expressed, as a function of time, as a summation of many phase-shifted optical pulses. Given that the US column is composed of many such layers, each of width $\Delta z = v_a \Delta t$, the detected pulsed fluorescence light can be written as

$$I_{\text{fluor}}(t) = \sum_{j=1}^m P(z) \cdot O(t - j\Delta t), \quad (1)$$

where $z = v_a j \Delta t$, and Δt is a time delay of the acoustic field, related to the number of steps m along the US column. $O(t)$ is an optical pulse from a given layer whose temporal profile is imposed by the ultrasonic excitation pulse. The profile $P(z)$ represents the optical intensity distribution along the acoustic axis as a result of the combined acoustical and optical characteristics along the ultrasonic column.

In a pulsed/tone-burst USMFT experiment, as the US is focused immediately in front of the target, the size of the target along the acoustic axis can be considered as an aperture of a virtual photo detector placed at the same position. One can therefore consider the profile $P(z)$ that contributes to the detected fluorescent signal as a combination of the acoustic and optical profiles and the size of the fluorescent target. We propose a simple expression relating the optical and acoustic properties to the profile $P(z)$, which can be expressed as

$$P(z) = P_{\text{us}}(z) \cdot P_{\text{ex}}(z) \cdot P_{\text{fluor}}(z), \quad (2)$$

where $P_{\text{us}}(z)$ is the axial pressure profile of the US, $P_{\text{ex}}(z)$ is the light intensity profile along the ultrasonic column, and $P_{\text{fluor}}(z)$ is the fluorescent profile. In the case of a transparent medium, $P_{\text{ex}}(z)$ represents the profile of the illumination; in the case of a scattering medium, $P_{\text{ex}}(z)$ represents a Gaussian profile that has been broadened by light scattering. In this simple model, we

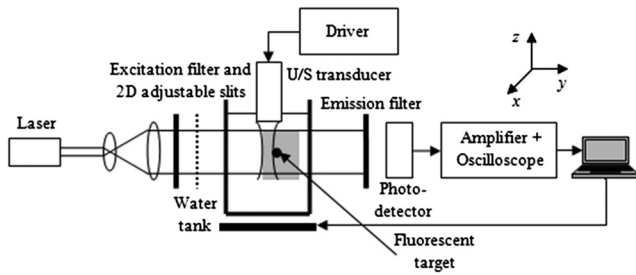


Fig. 2 Experimental setup.

assume that the profiles can be treated separately,²³ although inevitably there will be some dependence. To demonstrate the trends of experiments, such as the relationship between object size and acoustic wavelength, this model has been shown to be reliable.^{20,21} In a simplified form, $P_{us}(z)$ and $P_{ex}(z)$ can be represented as a Gaussian distribution, since a focused US transducer is usually used, and a narrow (1 mm-diameter) light beam illuminates the scattering medium. Profile $P_{fluor}(z)$ is related to the fluorophore distribution in the target. For example, in Fig. 1, the fluorescent target is represented as a top-hat profile, i.e., the fluorophore is uniformly distributed in the target and is zero outside.

3 Experimental Configuration

The experimental setup is shown in Fig. 2. An expanded HeNe ($\lambda = 632.8$ nm, $P = 20$ mW) laser illuminates the sample, and a photomultiplier tube (PMT, Hamamatsu H5783-20) is

employed as a detector. Filters from a fluorescent filter kit (Edmund Optics NT67-010) are used as an excitation filter (604 to 644 nm) and an emission filter (672 to 712 nm). Although a HeNe laser is employed, an excitation filter was still used in this experiment as a precautionary step to avoid any unwanted light from the pump source of the laser or from external sources. A signal generator (Tektronix AFG3022B) and a RF power amplifier (Amplifier Research 150A100B) are employed to drive a focused 1 MHz U/S transducer (Olympus Panametrics V314 NDT, 2.54 cm focal length). The US is focused at a position close to, but not at, the fluorescent object. This serves two purposes, first to ensure that the US field is not distorted by the target, which is not acoustically matched to the background medium. Second, it has been shown experimentally by other research groups^{10,14} that a higher SNR can be achieved using this configuration.

A 15- by 10- by 12 cm (XYZ) water tank sits on a computer-controlled XYZ motorized stage (Standa 8MT175-50). The signal from the PMT is fed into an amplifier (Mini-circuits ZFL-500LN+) before going to an oscilloscope (Tektronix TDS2024B 8 bit ADC) and subsequent storage on a PC. In all experiments, the fluorophore is Alexa633 (Invitrogen concanavalin A, Alexa Fluor 633 conjugate).

The system was used to investigate the effect that object size along the acoustic axis has on the modulation depth of the detected signal. To aid understanding and achieve better SNR, initial experiments were carried out in clear water before progressing to a scattering medium. Fluorescent objects of different dimensions were used as test targets (Fig. 3). Objects

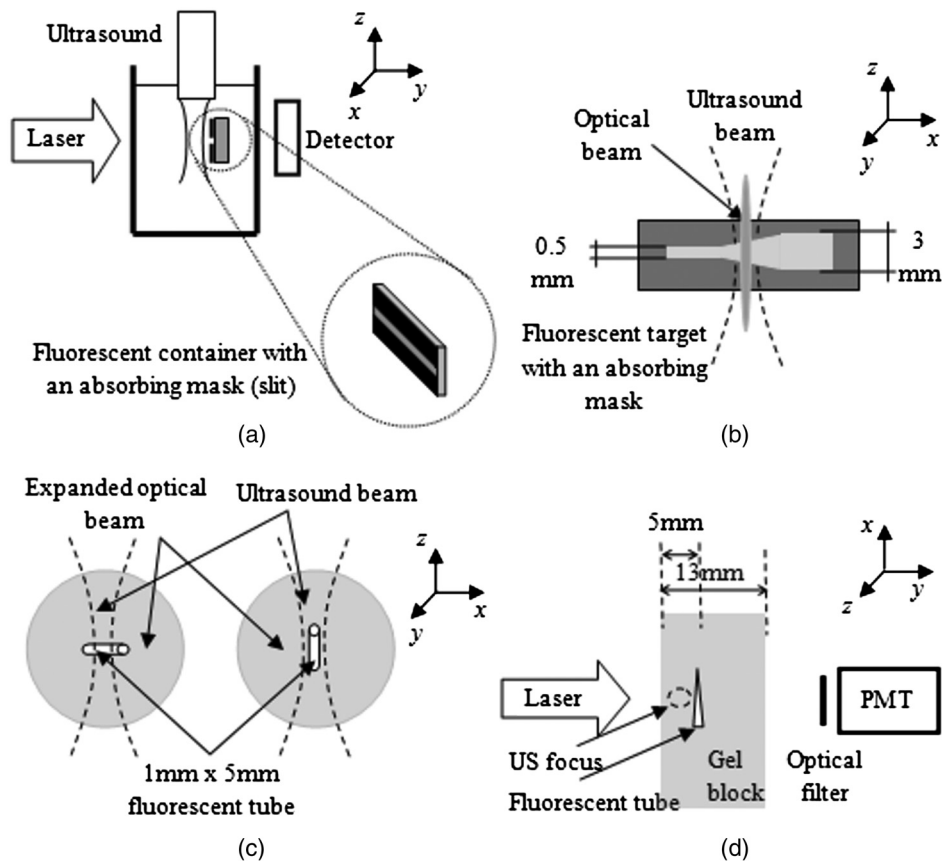


Fig. 3 (a) Target with slit masks (object 1). (b) Target with different profile (object 2). (c) Experimental arrangement with 1- by 5 mm fluorescent tube (object 3). (d) Fluorescent tube in a scattering gel block (object 4).

1 and 2 in Fig. 3(a) and 3(b) used a 12.5- by 3.5- by 5.2 mm (XYZ) (light path 1 mm) glass cuvette (Helma 110-OS) filled with fluorophore whose input face was covered with a black mask. In object 1 [Fig. 3(a)], the mask had a transparent slit which was used to simulate fluorescent objects of different sizes. In object 2 [Fig. 3(b)], the mask had a width of 0.5 mm at one end and tapered over a distance of 5 mm to a width of 3 mm at the other. Object 3 [Fig. 3(c)] was a 5 mm-long clear polyamide tube with 1 mm diameter containing fluorophore which was placed either vertically or horizontally. Object 4 [Fig. 3(d)] was a conical tube with the longest diameter of 1.8 mm and the shortest diameter of 0.4 mm, which was embedded in a 22- by 13- by 30 mm (XYZ) scattering agarose gel containing polystyrene microspheres ($\mu_s \sim 15 \text{ cm}^{-1}$ and $g = 0.93$). No additional absorption was added to the gel, so we assumed that the absorption coefficient of the gel was comparable to that of water ($\mu_a = 3 \times 10^{-3} \text{ cm}^{-1}$ at $\lambda = 632 \text{ nm}$ (Ref. 24) and could be neglected. It should be noted that for these early experiments the scattering coefficient was lower than that typically observed in body tissue (typically 100 cm^{-1}).

In all cases, the optical beam was modified so that it covered the region of interest. In the experiments with objects 1 and 3 [Fig. 3(a) and 3(c)], the laser beam was expanded to a diameter of 20 mm. In the case of object 2 [Fig. 3(b)], the expanded laser beam was truncated by a 1 mm vertical slit to produce a vertical sheet of light that probed a region with a different object width along the x axis. Beam expansion was not necessary with object 4, as it was embedded in a scattering medium. Each experimental pulse was averaged by the maximum 128 times on the oscilloscope, and this process was repeated 400 times at each location to provide a single averaged value. In all the scanning experiments, the scanning step was set to 0.5 mm. The power spectral density of the average detected signal was then calculated using the Auto Power Spectrum VI function in LABVIEW, which can be expressed as

$$\text{Power Spectrum} = \frac{\text{FFT}^*(\text{signal}) \times \text{FFT}(\text{signal})}{n^2}, \quad (3)$$

where n is the number of points in the signal ($n = 2500$ in this experiment) and $*$ denotes the complex conjugate. The magnitude of the spectrum was then summed over a 400 KHz bandwidth around the acoustic central frequency.

An acoustic frequency of 1 MHz (10-cycle tone burst) was used in experiments with clear water, while 1, 1.5, and 2 MHz (10 cycle tone-burst) were applied in scattering gel. A 10-cycle tone burst was selected, as it provides better SNR compared to both CW and single-cycle tone-burst US. Compared to a single-cycle tone-burst, a narrow bandwidth can be used for detection. Compared to a CW system, a higher peak power can be achieved, and also the effects of electromagnetic radiation (US excitation being picked up at the PMT) can be removed due to the time difference between US excitation and optical detection. A 10-cycle tone burst is relatively long ($\sim 15 \text{ mm}$) in terms of obtaining a significant improvement in axial resolution. However, this does not affect the trends and main conclusions of this work. Figure 4 shows the acoustic pressure from the 1 MHz transducer, which was excited by a 10-cycle, 1 MHz tone burst. The pressure was measured by a 1 mm-diameter needle hydrophone (Precision Acoustics Ltd 1705). From these data, we measured the transducer response to tone-burst excitation to be a 400 KHz-wide band pass filter

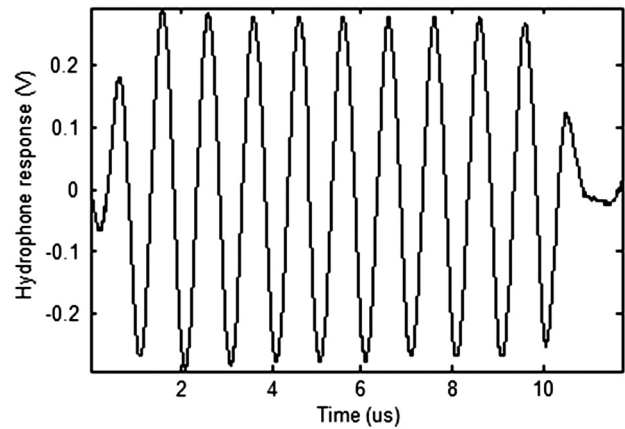


Fig. 4 (a) Simulated modulated signals for 1 MHz single-cycle tone-burst US and Fourier transform. (b) Ten-cycle 1 MHz tone burst as measured by hydrophone.

centered at the US frequency. The 400 KHz bandwidth was used in all the experiments to capture most ($\sim 98\%$) of the signal energy modulated by the 10-cycle tone-burst acoustic source. These values are used in the associated simulations.

4 Results

Experiments and simulations were initially carried out in clear water (Sec. 4.1) to ensure relatively high SNR and to better understand the relationship between the properties of the acoustic pulse and the dimensions of the object. Section 4.2 presents experimental and simulated images of object 4 embedded in a scattering gel block obtained using different US frequencies.

4.1 Clear Water

4.1.1 Object 1

The experiment investigated the effect of four slit widths (0.75, 1.5, 2.25, and 3 mm) on the detected signals and also verified the simple model employed. The optical profiles along the acoustic axis $P(z)$ used in the model for the different slits sizes are shown in Fig. 5, column 1. The normalized simulated and experimental US modulated fluorescence detected pulses are shown in Fig. 5, columns 2 and 3, respectively. There is good agreement between the shape of the simulated and experimental signals. As the US pulse propagates along the acoustic axis, fluorescent pulses are generated which propagate to the detector. Depending on the size of the slit, the fluorescent pulses that are produced as the acoustic pulse propagates may sum constructively or destructively to produce received pulses of different shapes and magnitudes. In the first row where the profile (0.75 mm) is half of an acoustic wavelength (1.5 mm), the ultrasonic pressure pulse is imposed on the USMFT signal, as the small slit size means that there is little opportunity for destructive summation of the fluorescent pulses to occur. When the profile is equal to the acoustic wavelength (row 2), the delays introduced into the pulses at each point mean that significant destructive interference occurs between the fluorescent pulses that arrive at the detector. It should be noted that at the beginning and end of the pulse there is less destructive interference, because these positions correspond to first-arriving and last-arriving pulses, which have no other pulses with which to interfere.

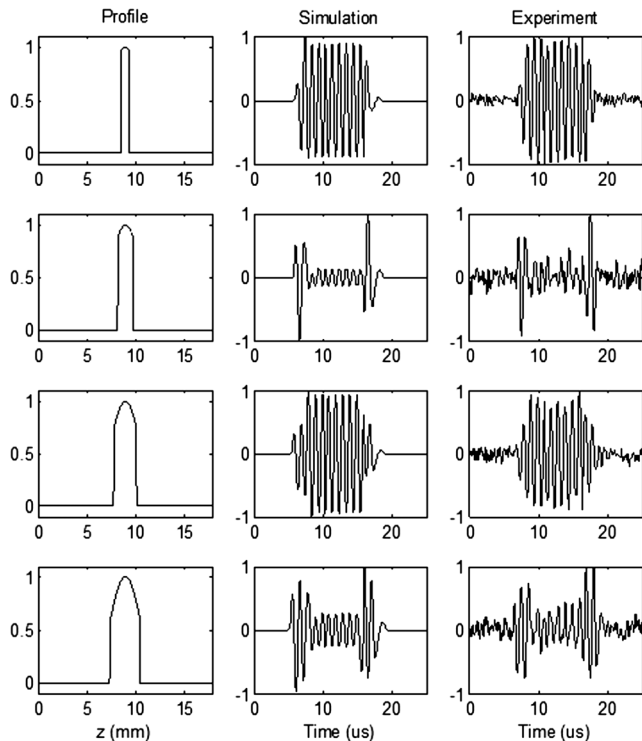


Fig. 5 Simulated (column 2) and experimental (column 3) results of pulsed USMFT signals for different fluorescent profiles (column 1): rows 1 to 4 correspond to fluorescent profiles of 0.75, 1.5, 2.25, and 3 mm. All signals were normalized by their maximum absolute values. Column 1 shows $P(z)$ used in the model to obtain the simulated data; z is defined in Fig. 2.

This pattern repeats for slit widths of 2.25 mm (1.5 acoustic wavelengths, row 3) and 3 mm (2 acoustic wavelengths, row 4).

4.1.2 Object 2

In this experiment, object 2 shown in Fig. 3(b) was scanned along the x direction. The mask includes three regions: the left region has a constant 0.5 mm transparent width (profile along z axis), whereas the right has a constant 3 mm transparent width (profile along z axis). The middle region produces a linear increase in profile (z axis). Object 2 was used to demonstrate the change in the modulated signal as the fluorescent profile is gradually increased from 0.5 to 3 mm. In this experiment, the laser beam was expanded (x - z dimensions) and truncated in the x dimension to produce a vertical thin sheet of light (1 mm), which could probe different widths of the object. The beam was then aligned in the middle of theinsonified focus region. Both modulated (AC) and unmodulated (DC) fluorescent light were detected. Figure 6(a) shows the experimental AC and DC traces from object 2. Figure 6(b) shows simulated AC traces with and without shot noise (shot noise was added in proportion to the square root of the DC light level).

It is clear that the DC and AC signal traces behave differently when the width of the fluorescent profile is increased. As anticipated, the DC line scan increased linearly as object 2 was scanned laterally, and the width of the profile increased from 0.5 to 3 mm. At either end of the object, both the AC and DC signals remained constant as the profiles were constant. However, the AC signal at the constant width of 0.5 mm was larger than that at 3 mm. Moreover, AC signals within the

middle region (0.5 to 3 mm) showed a minimum (at a width of 1.5 mm) and two maxima (at widths 0.75 and 2.25 mm). This can be explained by a discussion similar to the results for object 1. For maxima, the fluorescent pulses generated constructively sum at the detector, whereas the minima are due to destructive summing of the generated pulses. There is a good agreement in the trends of the experiments and the simulations. The SNR is relatively high, as water was used as the medium, and so the two simulated AC traces are similar. The only noticeable difference was when $x > 7$ mm, when the object became larger and contributed more shot noise.

4.1.3 Object 3

Another demonstration was carried out using object 3, which is imaged at the same position in two orientations (vertical and horizontal). Figure 7 shows AC and DC signal traces when object 3 was scanned laterally (x axis) in the two orientations. Although the DC signals are similar in both cases, an AC signal is detectable only when the object was oriented horizontally. This is because the width (1 mm) in the horizontal measurement was smaller than an acoustic wavelength, and no significant destructive interference of fluorescent pulses occurred. In the case where the object was aligned vertically, the width was 5 mm, allowing cancellation of fluorescent pulses to occur.

The results in Fig. 7 show that the modulation depth (ratio of modulated fluorescent signal to unmodulated fluorescent signal) is around 10^{-4} (compensating for the additional gain in the AC channel). This modulation depth is within the range that was predicted by Ref. 10. In theory, for an AC signal of $22.5 \mu\text{V}$ on a DC background of 6.4 mV and for our system parameters, the SNR is $\sim 5 \times 10^{-4}$, with shot noise dominating. The additional averaging that took place allowed a detectable signal to be obtained (the SNR became ~ 25.6 after 128×400 averaging).

4.2 Scattering Gel

Having demonstrated the basic principles in a nonscattering medium where the SNR is relatively high, a fluorescent object [Fig. 4(d)] embedded in a scattering gel was investigated. In this case, the beam expander was removed from the setup in Fig. 3 to deliver more light into the US focal zone. In this experiment, object 4 was scanned laterally (x axis) three times at three different US frequencies (10-cycle bursts of 1, 1.5, and 2 MHz). Simulated and experimental DC and AC traces are shown in Fig. 8.

The DC light level gradually increased with increasing x , as anticipated from a conical object, and then decreased as the US focus reached the edge of the object and moved away. As expected from the results in the nonscattering medium, the US-modulated fluorescence signal depended on the size of the fluorescent object and the modulation frequency of the US. Similar to the results shown for object 2 (Fig. 6), simulated results with and without shot noise are shown in Fig. 8(a) and 8(b), respectively. In the absence of shot noise [Fig. 8(a)], the simulations showed that the detected AC signals were proportional to the size of the object and the acoustic wavelength. Adding in the effects of shot noise [Fig. 8(b)] provided trends in the line-scans that had good agreement with those of the experimental results in Fig. 8(c) in terms of the number and relative size of the peaks in the line scan.

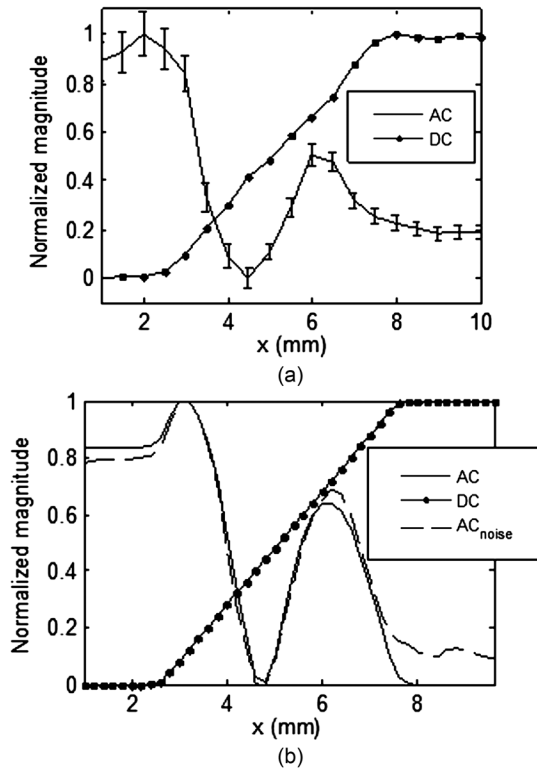


Fig. 6 AC and DC line scans of object 2. (a) Experimental results. (b) Simulated results. All line scans were normalized by their maximum absolute values.

As higher frequencies correspond to shorter wavelengths, the AC trace from the 2 MHz ultrasonic pulse oscillated faster than that from the 1- and 1.5 MHz pulses. Because the diameter of object 4 varied from 0.4 to 1.8 mm, with 1 MHz acoustic excitation, the trough in the AC image was at a diameter of ~ 1.5 mm, corresponding to one acoustic wavelength. Similarly, the trough in the 1.5 MHz USMFT image corresponded to a diameter of ~ 1 mm (one acoustic wavelength), and the maximum peak in the 2 MHz induced image corresponded to a diameter of ~ 1.125 mm (1.5 acoustic wavelengths). As the US transducer focal zone diameter was approximately 1 to 2 mm,²⁵ there was some averaging of the signal returned from the focal zone.

5 Discussion

The main aim of the paper was to investigate the effect of fluorescent object size and US frequency on the images obtained in pulsed USMFT. This is a useful fundamental investigation,

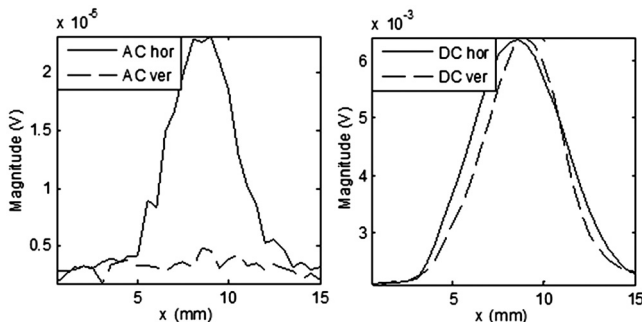


Fig. 7 Experimental 1-D AC and DC images of object 3.

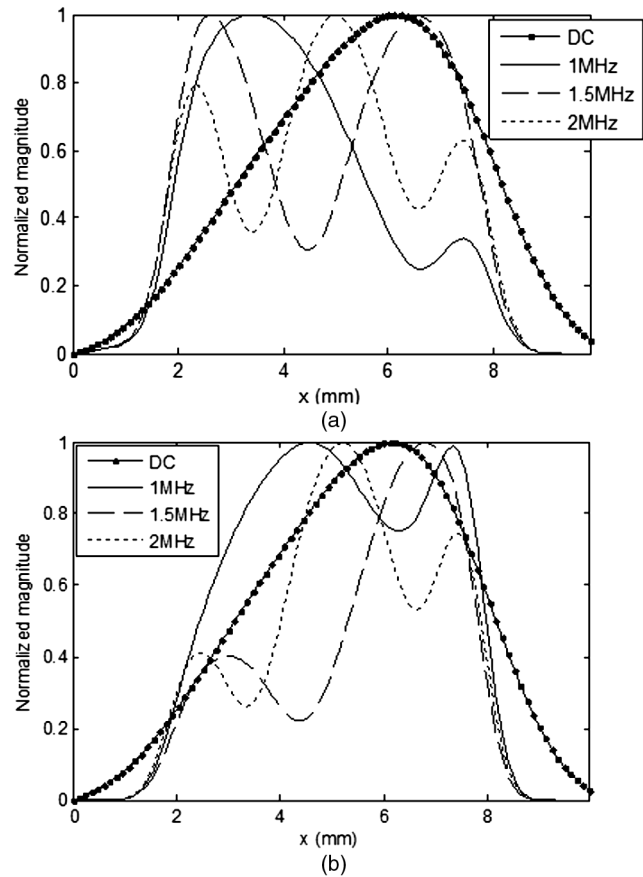


Fig. 8 Line scans of a fluorescent object 4 embedded in a scattering gel [noise free simulation (a) simulation noise added (b) experiment (c)] with 1-, 1.5-, and 2 MHz US. Line scans were normalized by their own maximum values.

because all systems to date have implemented CW US, and so these effects have not yet been considered. Pulsed US offers advantages in terms of allowing high peak pressures while remaining within safety limits and also enabling axial resolution along the acoustic axis to be obtained using time-gating.

All results showed that the detected USMFT signal depends on the size of the fluorescent target and the frequency of the US. If the object is of the order of an acoustic wavelength, then the US-modulated fluorescent pulses that propagate to the detector

are likely to cancel at the detector plane and produce a signal of relatively low amplitude. If the object is an odd number of half wavelengths wide, then the pulses will produce a larger detected signal due to more constructive interference occurring.

In the simulated data, a simple convolution model of a pulsed USMOT signal demonstrated by Huynh and colleagues^{20,21} was employed to predict the optical excitation signal at the surface of a fluorescent target. The simulation is simple because it neglects the effects of optical speckle and treats the fluorescent object as a planar object with different widths. The experimental results showed good agreement with the simulations for targets in a transparent medium (clear water) and scattering gel phantom (agarose gel mixed with 1.6 μm polystyrene microspheres). As discussed in more detail elsewhere (Ref. 21), the model could benefit from several improvements, such as more accurate estimation of the optical profile $P_{\text{ex}}(z)$ at the fluorescence object and taking into account the 3-D nature of the object and US focal zone. Rather than refine this simple model, we would implement a Monte Carlo simulation of light propagation as described elsewhere.⁸ However, the simulation serves a purpose in allowing the trends of USMFT to be predicted and an intuitive understanding of the detected signals to be obtained.

Although the model was developed primarily for the case of USMFT in scattering media, it is interesting to note that the results can also predict the trends of experiments carried out in clear water, where classic acousto-optic theory is valid. The fluorescent target in these experiments was placed closely (<1 mm) after the US focal zone which falls within the Fresnel region (near field distance $\lambda_{\text{us}}^2/4\lambda$, with λ_{us} and λ the US wavelength and the optical wavelength, respectively). According to Refs. 26–28, the near-field pattern is periodic with the frequency of the sound and moves with the progressive sound wave. In addition, the near-field light intensity diffracted by an ultrasonic wave with frequency Ω is

$$I(x, Y, z, t) = CI_i \left\{ 1 + 2 \sum_{n=1}^{\infty} J_n[2v_{x,z} \sin(2n\pi Y)] \times \cos[n(\Omega t + \Phi_{x,z} + \varphi)] \right\}, \quad (4)$$

where I_i is the incident laser intensity, C is a constant, J_n is the n th-order Bessel function of the first kind, $v_{x,z}$ and $\Phi_{x,z}$ are, respectively, the effective Raman-Nath parameter and the effective phase of the ultrasonic field along the projection path, φ is the initial phase of the ultrasonic wave, and Y is a normalized parameter defined as

$$Y = (y - L) \times \lambda / (2n_0 \lambda_{\text{us}}^2), \quad (5)$$

where L is the interaction length between the ultrasonic field and the light and n_0 is the refractive index of the medium.²⁸

In our experimental parameters ($y - L < 1$ mm, $\lambda = 632.8$ nm, $\lambda_{\text{us}} \sim 1.5$ mm, and $n_0 \sim 1.33$), Y becomes very small ($\sim 10^{-4}$). Hence, the Bessel term in Eq. (4) has a negligible contribution from orders >1 (e.g., Fig. 4 in Ref. 27). This subsequently simplifies the AC component of the optical intensity to an excitation signal on whose temporal profile is imposed the profile of the ultrasonic excitation pulse. As the US traverses the medium, a series of near-field optical signals are generated, which excite fluorescence pulses, which propagate and sum at the detector. This is similar to the basis of our simple convolution model, and hence the model is able to predict the trends in

clear water as well as scattering media. It is therefore important when interpreting pulsed USMFT data to take into account the relative size of the object and the modulation frequency applied. Although this varying signal could be considered a hindrance, it may be possible to use it to extract more information by probing an object with multiple acoustic frequencies. For example, for a single fluorescent object embedded within a medium, a single-frequency system may be able to map a two-dimensional (2-D) image by performing a 2-D scan of the US. The experiment is not only more time consuming, but also provides low axial resolution which is mainly defined by the focal zone of the US transducer. By performing a multifrequency experiment, one could potentially determine the depth of the object based on the relative change of the detected signal in different frequencies. In another scenario, where a sample contains multiple objects with different sizes, the multifrequency method potentially detect all the objects by scanning the US, whereas a single-frequency system may produce only images of objects whose sizes are most responsive to the ultrasonic wavelength. For inversion algorithms, the additional information provided by the multifrequency approach may allow for better posed reconstruction.

Although the experimental signals provide good match with the model, the SNR is still very low and the acquisition time is high. This is a disadvantage, as the safety threshold cannot be exceeded in practical applications, and also photobleaching of the fluorophore needs to be considered. To increase the SNR, microbubbles could be used to produce a bigger change in the optical properties within the insonified region. With improvements in SNR, the tone burst can be shorter in duration, resulting in better axial resolution. The effects observed on the detected signal caused by the summation of fluorescent pulses

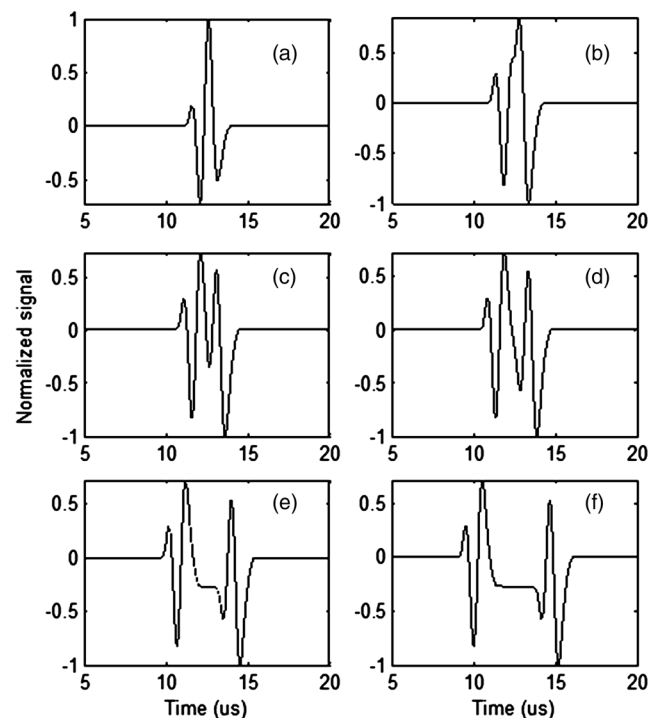


Fig. 9 Simulated results of single-cycle tone-burst USMFT signals for different fluorescent profile widths 0.75 mm (a) 1.5 mm (b) 2.25 mm (c) and 3 mm (d). All the signals were normalized by their maximum absolute values. These signals show the same summation trends as in Fig. 5.

propagating to the detector will still be present and need to be taken into account. These have previously been observed experimentally for a single-cycle tone burst and coherent light detection.²¹ As an example, Fig. 9 shows simulated data for the same parameters as those shown in Fig. 5 except for a single-cycle tone burst. Less destructive interference is observed for the object sizes considered in the experiment [Fig. 9(a)–9(d)] owing to the shorter timescales involved in the summation, but significant broadening and distortion of the detected signal can still be observed. The data are shown normalized to aid visualisation, but the peak amplitudes for Fig. 9(b)–9(d) are approximately 60% of that shown in Fig. 9(a). Figure 9(e) and 9(f) shows that as the object size increases further, the distortion becomes even greater. This effect is scalable and has been observed for smaller objects at higher acoustic frequencies (10 MHz) in coherent light.²¹

6 Conclusion

The first pulsed US-modulated fluorescence tomography system has been demonstrated, and the effects of fluorescent target size and acoustic frequency on the detected signals have been investigated. As the acoustic pulse propagates through the medium, fluorescent pulses are generated which propagate to the detector. Depending on the size of the object and the acoustic frequency, these pulses can sum either constructively or destructively at the detector. When the object is an integer number of acoustic wavelengths wide, the pulses sum destructively. When the object is an odd number of half wavelengths wide, the pulses sum constructively and produce a comparatively higher signal. This has been demonstrated experimentally and using a simple simulation of the pulsed USMFT process. This effect needs to be taken into account, as it will produce image artifacts. However, probing a sample with multiple acoustic frequencies may allow additional information to be obtained.

Acknowledgments

This work was supported by the Biotechnology and Biological Sciences Research Council (BBSRC) UK (BB/F004826/1 and BB/F004923/1). H. Ruan was funded by the China Scholarship Council.

References

- J. R. Lakowicz, *Principles of Fluorescence Spectroscopy*, Springer, New York (2006).
- D. Razansky et al., “Multispectral opto-acoustic tomography of deep-seated fluorescent proteins *in vivo*,” *Nat. Photon.* **3**(7), 412–417 (2009).
- L. Li et al., “Photoacoustic imaging of lacZ gene expression *in vivo*,” *J. Biomed. Opt.* **12**(2), 020504 (2007).
- C. A. DiMarzio and T. W. Murray, “Medical imaging techniques combining light and US,” *Subsurface Sens. Technol. Appl.* **4**(4), 289–309 (2003).
- S. Sakadzic and L. V. Wang, “High-resolution US-modulated optical tomography in biological tissues,” *Opt. Lett.* **29**, 2770–2772 (2004).
- S. Kothapalli and L. V. Wang, “Ex vivo blood vessel imaging using US modulated optical microscopy,” *J. Biomed. Opt.* **14**(1), 014015 (2009).
- J. Li and L. V. Wang, “US-modulated optical computed tomography of biological tissues,” *Appl. Phys. Lett.* **84**(9), 1597–1599 (2004).
- Q. Liu, S. Norton, and T. Vo-Dinh, “Modeling of nonphase mechanisms in ultrasonic modulation of light propagation,” *Appl. Opt.* **47**(20), 3619–3630 (2008).
- L. V. Wang, “Mechanisms of ultrasonic modulation of multiply scattered coherent light: a Monte Carlo model,” *Opt. Lett.* **26**, 1191–1193 (2001).
- B. Yuan, J. Gamelin, and Q. Zhu, “Mechanisms of the ultrasonic modulation of fluorescence in turbid media,” *Appl. Phys.* **104**(10), 103102 (2008).
- M. Kobayashi et al., “Fluorescence tomography in turbid media based on acousto-optic modulation imaging,” *Appl. Phys. Lett.* **89**(18), 181102 (2006).
- D. Hall, “Feasibility of dual optics/US imaging and contrast media for the detection and characterization of prostate cancer,” Annual Report for U. S. Army Medical Research and Materiel Command, Fort Detrick, MD, acc. no. ADA503452 (2009).
- K. Krishnan et al., “A theory for the ultrasonic modulation of incoherent light in turbid medium,” *Proc. SPIE* **6009**, 147–158 (2005).
- B. Yuan and Y. Liu, “US-modulated fluorescence from rhodamine B aqueous solution,” *J. Biomed. Opt.* **15**(2), 021321 (2010).
- D. J. Hall et al., “Detection of US-modulated photons and enhancement with US microbubbles,” *Proc. SPIE* **7177**, 71771L (2009).
- J. E. Honeysett, E. Stride, and T. S. Leung, “Microbubble enhancement of US-modulated optical sensing with incoherent light,” *Proc. SPIE* **7899**, 789919 (2011).
- B. Yuan, “US-modulated fluorescence based on a fluorophore-quencher-labeled microbubble system,” *J. Biomed. Opt.* **14**(2), 024043 (2009).
- M. J. Benchimol et al., “Ultrasound-quenchable fluorescent contrast agent: experimental demonstration,” in *Optical Molecular Probes, Imaging and Drug Delivery*, OSA Technical Digest (CD), Optical Society of America, Washington, paper OMD2 (2011).
- B. Yuan et al., “Microbubble-enhanced US-modulated fluorescence in a turbid medium,” *Appl. Phys. Lett.* **95**(18), 181113 (2009).
- N. T. Huynh et al., “Application of a maximum likelihood algorithm to US modulated optical tomography,” *Proc. SPIE* **7899**, 78991C (2011).
- N. T. Huynh et al., “Application of a maximum likelihood algorithm to ultrasound modulated optical tomography,” *J. Biomed. Opt.* **17**(2), 026014 (2012).
- K. Zell et al., “Acoustical properties of selected tissue imaging materials for US imaging,” *Phys. Med. Biol.* **52**(20), N475–N484 (2007).
- D. A. Boas et al., “Scattering and wavelength transduction of diffuse photon density waves,” *Phys. Rev. E* **47**(5), R2999–R3000 (1993).
- R. M. Pope and E. S. Fry, “Absorption spectrum (380–700 nm) of pure water. II. Integrating cavity measurements,” *Appl. Opt.* **36**(33), 8710–8723 (1997).
- Ultrasonic transducers technical note, Olympus Panametrics, 2006, <http://www.olympus-ims.com/en/pdf-library/157-catId.268435489.html> (18 September 2012).
- H. M. Colbert and K. L. Zankel, “Light diffraction by ultrasonic waves: Fresnel region,” *J. Acoust. Soc. Am.* **35**(3), 359–363 (1963).
- B. D. Cook, “Measurement from the optical nearfield of an ultrasonically produced phase grating,” *J. Acoust. Soc. Am.* **60**(1), 95–99 (1976).
- G. Yao and L. H. Wang, “Full-field mapping of ultrasonic field by light source-synchronized projection,” *J. Acoust. Soc. Am.* **106**(4), L36–L40 (1999).